© 1998 The Chemical Society of Japan

Accounts

Solitons, Polarons, and Excitons in Quasi-One-Dimensional Halogen-Bridged Transition Metal Compounds

Hiroshi Okamoto* **and Masahiro Yamashita*,†**

Department of Applied Physics, The University of Tokyo, Hongo, Bunkyo-ku, Tokyo 113-8656

†Graduate School of Human Informatics and PRESTO, Nagoya University, Chikusa-ku, Nagoya 464-8601

(Received March 20, 1998)

We report the photogeneration of solitons and polarons in the quasi-one-dimensional (1-D) halogen (X)-bridged metal (M) compounds (simply abbreviated as the MX chain compounds). The most significant feature of this system is the remarkable tunability of the charge density wave (CDW) ground states. By substituting the metals (M = Pt, Pd, and Ni), the bridging halogens (X = Cl, Br, and I), the ligand molecules and the counter anions surrounding the 1-D chains, the amplitude of CDW, the optical gap energy, and the degeneracy of CDW can be widely controlled. On the basis of these controls, we have investigated the nature of photoexcited states. By comparing the results of photoinduced absorption (PA), ESR and photoinduced ESR measurements in the degenerate CDW states with those in the non-degenerate CDW states, we clearly characterized the photoinduced gap states as solitons and polarons. In the compounds having relatively large optical gap energies (E_{CT}), spin-solitons and polarons are photogenerated. From a comparison of the excitation profiles of the PA signals with those of the luminescence of the self-trapped exciton (STE), it was demonstrated that the luminescence process strongly competes with the dissociation to spin–soliton pairs. An analysis of the temperature dependence of the luminescence decay time revealed that the conversion from an STE to a solitonic state occurs through a finite potential barrier, the magnitude of which depends on degeneracy of CDW. With decrease of E_{CT}, the nature of the photoexcited states changes considerably; photogenerations of charged-solitons are observed instead of spin–solitons and the STE luminescence is remarkably quenched. While referring to the theoretical expectations based upon the Peierls–Hubbard model, we will discuss the overall view of the relaxation process of the photoexcited states related to solitons, polarons, and excitons in the MX compounds.

Elementary excitations associated with lattice instability in the 1-D half-filled electronic systems have attracted much attention from both theoretical and experimental point of views. It has been revealed that the concepts of solitons[1] and other nonlinear excitations are essential for understanding the optical and magnetic properties as well as the transport properties of the 1-D materials such as conjugated polymers.[2] Subsequently, the halogen (X)-bridged metal (M) complexes (or equivalently the MX chain compounds) have provided a unique opportunity to study the instability of the 1-D Peierls–Hubbard system. A number of studies have been reported concerning the electronic properties in 1-D MX chains.[3—37]

The MX chain compounds are represented as $[MA_2]$-$[MA_2X_2]Y_4$ (or simply $\{MA_2X\}Y_2$), where A and Y are the ligand and the counter anion, respectively. As schematically illustrated in Fig. 1, the $[MA_2]$ moieties are bridged by the halogen ions (X), and the hydrogen (H)-bonds between the amino-groups of the ligands (A) and the counter anions (Y) support the 1-D MX chains. The most notable feature of the MX chain compounds is the remarkable tunability of the electronic states.[6,15,17,20] The amplitudes of the CDW states can be controlled by replacements of the metals (M = Pt, Pd, and Ni), the bridging halogens (X = Cl, Br, and I), the

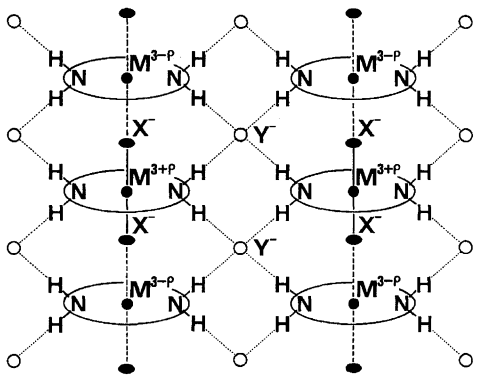

Fig. 1. Schematic structure of the halogen (X)-bridged metal (M) compound. Ligand molecules (A_2) are shown by ovals. Hydrogen-bonds are shown by the dotted lines.

ligand molecules (A = ethylenediamine, ethylamine, diaminocyclohexane, etc.) and the counter anions (Y^- = ClO_4^-, BF_4^-, Cl^-, Br^-, I^-, etc.) surrounding the 1-D chains.[17,20] In addition, the nondegenerate CDW states can be obtained in the hetero-metal compounds in which Pt and Pd ions arrange alternatively.[15,37] Such a control of the CDW states in the MX chain compounds allows us to make an advanced study of dynamics of the nonlinear excitations such as solitons and polarons.[21,37]

In this paper, first, we will report the photoinduced absorption (PA) spectroscopy and photoinduced ESR (PESR) measurements of the several typical MX chain compounds to characterize the photoinduced gap states. The definitive assignments of the PA and PESR signals to solitons and polarons can be obtained by comparing the results in the degenerate CDW states with those in the nondegenerate CDW states. Second, we will discuss the relaxation dynamics of the photoexcited states related to solitons, polarons, and excitons. Generation of soliton pairs or polaron pairs and their following nonradiative recombination is one of the main relaxation channels of the photoexcited states.[21,25,29,30,37] Another important relaxation channel of the photoexcited states is the luminescence process from a self-trapped exciton (STE).[3—6] The importance of these two relaxation channels depends on the gap energies, that is, the magnitude of the electron-lattice (e-l) interactions.[20,25] In the compounds having relatively large gap energies, the luminescence process competes with the generation process of the gap states. We will demonstrate that excitons are relaxed to solitonic states from a comparison between the excitation profiles of the STE luminescence and those of the gap states. Moreover, from an analysis on the temperature dependence of luminescence decay times, dynamical aspects of the conversion from an STE to a solitonic state will be reported. On the other hand, in the compounds with small gap energies, the luminescence process almost disappears, and the generation process of the gap states seems to become dominant. From the comparison of these experimental results with the theoretical expectations based upon the Peierls–Hubbard model,[38—47] we will discuss the overall view of the relaxation process of the photoexcited states in the MX chain compounds.

Contents of this paper are as follows. In Sect. 1, experimental details are described. In Sect. 2, we will review how to control the CDW states by the substitution of the constituent elements. After that, in Sect. 3, we will clarify the nature of photoinduced gap states and the relaxation process of the photoexcited states concerning solitons, polarons, and excitons. A summary is given in Sect. 4.

1. Experimental

The Pt compounds were synthesized in the same way as reported in Refs. 48, 49, and 50. The hetero-metal compounds with Pt and Pd were synthesized in the same way as reported in Ref. 51. In order to avoid the introduction of different halogen ions as impurities, we used as the starting reagents K_2PtCl_4 (K_2PdCl_4), $PtBr_2$($PdBr_2$), and PtI_2 for the chloro-, bromo-, and iodine-bridged Pt (Pd) compounds, respectively.

Polarized reflectivity spectra were measured in the same way as reported in Ref. 17. In the PA measurements for the visible region, probe lights obtained from a halogen–tungsten incandescent lamp were passed through the single crystal samples, and then the transmission lights were monochromized by a grating monochromator (JASCO CT25C). The change in the transmittance of the sample induced by the excitation lights was detected by a photomultiplier. In the infrared (IR) and near-IR region, a Fourier-transform infrared spectrometer (Nicolet system 800 or JASCO IR-8000) equipped with a HgCdTe or InSb detector was used for the measurements of the change of the transmittance. The details of the experimental procedures were reported elsewhere.[52]

ESR and photoinduced ESR measurements were performed by using the X-band ESR spectrometer (JEOL JES-RE3X).

Time-integrated luminescence spectra were measured by using a grating monochromator (JASCO CT25C) equipped by a Ge photodiode or PbS cell. Time-resolved luminescence spectra were obtained by using a synchronous scan streak camera or time-correlated single-photon counting, depending on the energy region.

As the excitations for the PA, PESR, and time-integrated luminescence measurements, we used the Ar ion laser and the light from a 75 W Xe lamp or a 650 W halogen lamp monochromized by using a grating monochromator (JASCO CT-10) or the band pass filters with band widths of ca. 40 nm. For the time-resolved luminescence measurements, the second harmonics of Ti-sapphire laser (3.2 eV) with the pulse width of 120 fs and the repetition of 76 MHz was used.

2. Control of the CDW States

In the MX chain compounds, the 1-D electronic state is composed of d_{z^2} orbitals of the metals and p_z orbitals of the bridging halogens, where the z axis is pararell to the MX chain. The ground state is expressed as the mono-valence state or the mixed-valence state (or equivalently the commensurate CDW state) as shown in Fig. 2 (A) and (B), respectively. Competition between the stabilization energy (E_s) of the d_{z^2} electrons due to the distortion of the bridging halogens and the Coulomb repulsion energy (U) on the metal site determines whether the ground state is the mono-valence state or the mixed-valence state.[53,54] Briefly, the Ni compounds have the mono-valence ground state,[55,56] while the Pt and Pd compounds have the mixed-valence state.[6,20] The recent Auger electron spectroscopy has revealed that the magnitude of U is about 5 eV in the Ni compounds,[33] which is much larger than that in the Pt or Pd compounds (0.5—2 eV).[15,42,44] Moreover, it has been demonstrated from the detailed optical

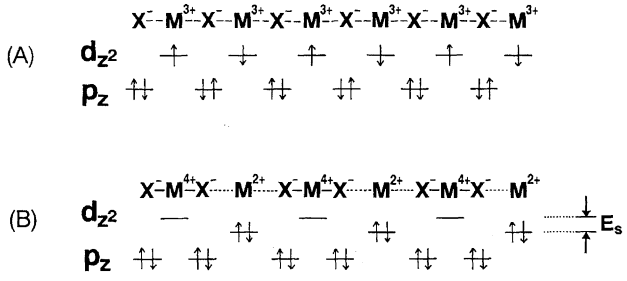

Fig. 2. Schematic electronic structure of the MX chain; (A): the mono-valence state, and (B): the mixed-valence (CDW) state.

and X-ray photoelectron spectroscopy that the Ni compounds are the so-called charge-transfer (CT) insulators.[33] This fact is consistent with the Zaanen–Sawatzsky–Allen scheme.[57] In this paper, we focus only on the Pt and Pd compounds in the CDW states. In the following, we will detail how to control the CDW states by substitution of the constituent elements.

2-1. Control of Amplitude of CDW. By replacing the metal (M = Pt, or Pd) and the bridging-halogen ion (X = Cl, Br or I), the Coulomb repulsion energy (U) on the metal site and the transfer energy (T) between the nearest neighbor metal sites are considerably changed, since the sizes of the orbitals are different among the respective metal ions (M) and halogen ions (X).[6,20] Thus, one expects to obtain a variety of compounds having the different bridging-halogen distortions Δ. Δ is defined as the displacement of the bridging-halogen ion from the midpoint between the neighboring two metal ions. From the analysis of crystal structures, in fact, the halogen distortion is closely correlated to the metal to metal (M–M) distance L, which is strongly dependent on the choice of the ligand (A) and the counter anion (Y) and simultaneously on the strength of the H-bond between A and Y,[20] as mentioned below.

In Table 1, the M–M distance L, the metal to halogen (M–X) distance l_1 and l_2 ($l_1 < l_2$), the halogen displacement Δ ($l_2 - l_1 = 2\Delta$), and the distortion parameter d ($d = 2\Delta/L$) are listed for the various kinds of halogen-bridged metal compounds.[58–64] In Fig. 3, the values of l_1 and l_2 are plotted as a function of L for the compounds with X = Cl and X = Br. The dotted line indicates $l_1 = l_2 = L/2$, which is a hypothetical line for the compounds with no bridging-halogen distortion. The deviation of l_1 and l_2 from the dotted line corresponds to a magnitude of the halogen displacement ($\Delta = (l_2 - l_1)/2$). The most notable feature of Fig. 3 is that the data points fall on almost the same lines according to the choice of the bridging-halogen ions (Br^- or Cl^-), while M, A, and Y are replaced. It indicates the strong correlation between Δ and L.

The typical MX chain compounds have ClO_4^- for the counter anion. The data of these compounds are shown by open marks in Fig. 3. The data of the compounds with halogen ions for the counter anion are plotted by solid marks in the same figure. By changing the counter anion from ClO_4^- to halogen ions, the H-bonds between the amino-groups of the ligands and the counter anions are strengthened, as ascertained by the IR and X-ray measurements.[17,65] Here, we will introduce the results of the IR measurements.[65] Figure 4 shows the IR spectra of $[Pt(chxn)_2][Pt(chxn)_2Br_2]Br_4$ and $[Pt(chxn)_2][Pt(chxn)_2Br_2](ClO_4)_4$ together with those of constituent elements of the compounds, cyclohexane and chxn for comparison. The structures peaked at 2850 and 2910 cm^{-1} were observed for all of the materials, so that these peaks are assigned to the C–H stretching mode of the cyclohexane moieties. A broad band was commonly observed in an energy range of 2800—3400 cm^{-1} except for the spectrum of cyclohexane molecule, which originates in the N–H stretching of the ligand; the N–H band shows a lower energy shift, ca. 180 cm^{-1} from chxn to $[Pt(chxn)_2][Pt(chxn)_2Br_2]$-

Table 1. The M–M Distance L, the M–X Distance l_1 and l_2 ($l_1 < l_2$), the Halogen Displacement Δ ($l_2 - l_1 = 2\Delta$), the Distortion Parameter d ($d = 2\Delta/L$), the CT Exciton Energy E_{CT}, and the Luminescence Energy E_{lm} for the Various MX Compounds
As for the lattice parameters (L, l_1, l_2, Δ), see Ref. 58 for No. 1, 4, 8, 12, 14; Ref. 59 for No. 2; Ref. 49 for No. 3; Ref. 60 for No. 5; Ref. 17 for No. 6, 11; Ref. 61 for No. 7; Ref. 62 for No. 9; Ref. 63 for No. 10; Ref. 64 for No. 13; Ref. 56 for No. 15; Ref. 55 for No. 16.

	Abbreviations	L(Å)	l_1(Å)	l_2(Å)	Δ(Å)	d	E_{CT} (eV)	E_{lm} (eV)
1. $[Pt(chxn)_2][Pt(chxn)_2Cl_2](ClO_4)_4$		5.730	2.314	3.416	0.511	0.190	3.20[a]	1.49[a]
2. $[Pt(en)_2][Pt(en)_2Cl_2](ClO_4)_4$	Pt–Cl–Pt	5.403	2.318	3.095	0.3885	0.144	2.73[b]	1.17[b]
3. $[Pt(chxn)_2][Pt(chxn)_2Cl_2]Cl_4$	2-D Pt–Cl–Pt	5.158	2.324	2.834	0.255	0.099	1.99[c]	0.90[d]
4. $[Pt(en)_2][Pt(en)_2Br_2](ClO_4)_4$–I	Pt–Br–Pt–I	5.493	2.487	3.006	0.2595	0.094	1.98[b]	0.78[b]
5. $[Pt(en)_2][Pt(en)_2Br_2](ClO_4)_4$–II	Pt–Br–Pt–II	5.695	2.487	3.208	0.3605	0.1266	2.40[e]	1.11[e]
6. $[Pt(chxn)_2][Pt(chxn)_2Br_2]Br_4$	2-D Pt–Br–Pt	5.372	2.490	2.882	0.196	0.073	1.40[f]	0.68[d]
7. $[Pt(en)_2][Pt(en)_2I_2](ClO_4)_4$	Pt–I–Pt	5.820	2.726	3.093	0.1835	0.063	1.38[b]	0.60[a,d]
8. $[Pt(chxn)_2][Pt(chxn)_2I_2]I_4$	2-D Pt–I–Pt						0.94[c]	—
9. $[Pd(en)_2][Pd(en)_2Cl_2](ClO_4)_4$		5.357	2.324	3.033	0.3545	0.130	2.05[a]	0.86[a]
10. $[Pd(en)_2][Pd(en)_2Br_2](ClO_4)_4$		5.407	2.911	2.496	0.2075	0.075	1.13[a]	0.40[a]
11. $[Pd(chxn)_2][Pd(chxn)_2Br_2]Br_4$	2-D Pd–Br–Pd	5.296	2.523	2.773	0.125	0.047	0.75[f]	—
12. $[Pd(en)_2][Pt(en)_2Cl_2](ClO_4)_4$	Pt–Cl–Pd	5.415	2.315	3.100	0.3925	0.145	3.22[g]	1.65[g]
13. $[Pd(en)_2][Pt(en)_2Br_2](ClO_4)_4$	Pt–Br–Pd	5.502	2.467	3.035	0.284	0.103	2.59[g]	1.54[h]
14. $[Pd(en)_2][Pt(en)_2I_2](ClO_4)_4$	Pt–I–Pd	5.866	2.678	3.188	0.255	0.087	2.28[i]	1.12[i]
15. $[Ni(chxn)_2Cl]Cl_2$		4.894	2.447		0	0	1.83[j]	—
16. $[Ni(chxn)_2Br]Br_2$		5.160	2.580		0	0	1.28[j]	—

a) Ref. 6, b) Present work (see Ref. 69), c) Present work, d) Ref. 20, e) Ref. 37, f) Ref. 17, g) Ref. 15, h) Present work (see Ref. 70), i) Present work (see Ref. 71), j) Ref. 33.

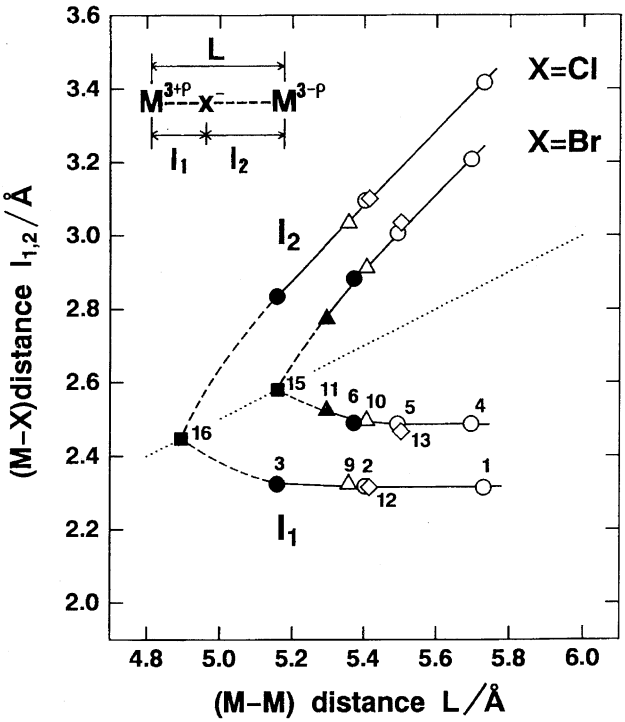

Fig. 3. The correlation between the M–M distance (L) and the M–X distance (l_1 and l_2). The numbers in this figure correspond to those in Table 1. The data of the homo-metal compounds are represented by circles for M = Pt, triangles for M = Pd, and squares for M = Ni, respectively. The data of the hetero-metal compounds with M = Pt and Pd are represented by diamonds. The open and filled marks indicate the compounds with Y = ClO_4 and Y = halogen, respectively.

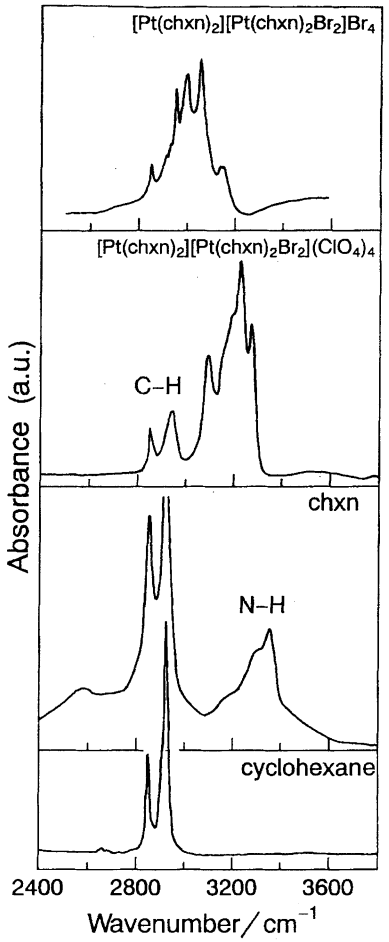

Fig. 4. IR spectra for cyclohexane, chxn, $[Pt(chxn)_2][Pt(chxn)_2Br_2](ClO_4)_4$, and $[Pt(chxn)_2][Pt(chxn)_2Br_2]Br_4$.

$(ClO_4)_4$ and ca. 250 cm^{-1} from $[Pt(chxn)_2][Pt(chxn)_2Br_2](ClO_4)_4$ to $[Pt(chxn)_2][Pt(chxn)_2Br_2]Br_4$. The energy shift of the N–H stretching mode is useful as a measure of the strength of the H-bond. The observed red shift indicates that the H-bond is strengthened by the replacement of Y = ClO_4 with Y = Br. Such a replacement of the counter anion induces the decrease of the M–M distance L. As seen in Fig. 3, the lengths L of the compounds with Y = halogen are relatively smaller than those of the compounds with Y = ClO_4.

On the other hand, the position of the bridging-halogen ion between the neighboring two metal ions (that, is the M–X distance l_1 and l_2) depends strongly on the choice of the bridging-halogen ion (X). As seen in Fig. 3, the shorter M–X distance l_1 is almost constant in the mixed-valence Pt or Pd compounds with the same bridging-halogen ion, even if the M–M distance L considerably changes. This constant value of l_1 is considered to be the distance where the nucleus potential for the bridging-halogen ion increases anharmonically, since l_1 is close to the sum of the ionic radii of the bridging halogen (Cl^-: 1.67 Å, Br^-: 1.82 Å[66,67]) and the metal (Pd^{4+}: 0.76 Å, Pt^{4+}: 0.77 Å[68]). Starting from the M^{3+}–X^- regular chain structure, the deviation of l_1 from the dotted line ($L/2$) corresponds to the amplitude of the halogen distortion Δ. Therefore, the constant values of l_1 introduces the limit of Δ. The decrease of L induces the decrease of the longer M–X distance l_2, and then necessarily induces the decrease of the halogen distortion ($\Delta = (l_2 - l_1)/2$). Thus, the decrease of L effectively suppresses the e-l interactions. At the same time, the decrease of L leads to the increase of transfer energy (T). Accordingly, with decrease of L, the electronic states become delocalized.

Another important effect of the H-bond to the electronic state manifests itself in the interchain interaction. In the mixed-valence Pt or Pd complexes with halogen for the counter anion, a direction of each halogen displacement is two-dimensionally ordered, as pointed out from the X-ray analysis.[17,20] The phases of the halogen distortions within each chain accord with one another in the *bc* plane, as shown below.

$$\begin{array}{l}
\cdots X^- - M^{4+} - X^- \cdots M^{2+} \cdots X^- - M^{4+} - X^- \cdots M^{2+} \cdots X^- - \\
\cdots X^- - M^{4+} - X^- \cdots M^{2+} \cdots X^- - M^{4+} - X^- \cdots M^{2+} \cdots X^- - \\
\cdots X^- - M^{4+} - X^- \cdots M^{2+} \cdots X^- - M^{4+} - X^- \cdots M^{2+} \cdots X^- -
\end{array}$$

(Figure 1 shows the compound having a 2-D ordering of CDW.) This is not due to the overlapping of the electronic states between the chains but to the interchain coupling through the tight network of the H-bonds between the amino-groups of the ligands and the counter halogen ions. Thus,

although the electronic states are still one-dimensional, a 2-D plane ordering of CDW is formed. However, in the compounds with ClO_4^- for the counter anion, such an ordering is not formed; the H-bond interchain coupling is weak and the crystal seems to be purely one-dimensional. The existence of a 2-D ordering of CDW provides serious modifications to the relaxation process of the photo-excited states, as discussed in Sect. 3 (3-4).

2-2. Control of the Degeneracy of CDW. The MX compounds have the doubly degenerate CDW ground states, which are expressed as

$$\text{---}X^-\text{–}M^{4+}\text{–}X^-\text{---}M^{2+}\text{---}X^-\text{–}M^{4+}\text{–}X^-\text{---}M^{2+}\text{---}X^-\text{–} \quad [A]$$
$$\text{–}X^-\text{---}M^{2+}\text{---}X^-\text{–}M^{4+}\text{–}X^-\text{---}M^{2+}\text{---}X^-\text{–}M^{4+}\text{–}X^-\text{---} \quad [B].$$

The difference of the phase of CDW between [A] and [B] is π. Such a degeneracy of 1-D CDW states will be modified in the MX chain compounds with 2-D ordered CDW mentioned in the previous subsection. In the 2-D ordered CDW state with the phase [A], it will cost a finite energy to convert one chain from [A] to [B].

Degeneracy of CDW states can be excluded more clearly by the metal alternation. By substituting a half of Pt ions with Pd ions, we can obtain the hetero-metal compounds where Pt and Pd ions are arranged alternatively.[59] In the hetero-metal compounds, the 1-D electronic state is composed of the 4d orbitals of Pd ions and the 5d orbitals of Pt ions. Since the energy level of 4d orbitals in Pd ions is lower than that of 5d orbitals in Pt ions, the CDW state is composed of Pd^{2+} ions and Pt^{4+} ions, as shown below.

$$\text{---}X^-Pt^{4+}\text{–}X^-\text{---}Pd^{2+}\text{---}X^-\text{–}Pt^{4+}\text{–}X^-\text{---}Pd^{2+}\text{---}X^-\text{–}$$

In this case, the CDW ground state is nondegenerate. The interrelation between the homo-metal compounds and the hetero-metal compounds is analogous to that between the *trans*-$(CH)_x$ and *cis*-$(CH)_x$.

The lattice parameters, L, l_1, and l_2 for the hetero-metal compounds are also plotted in Fig. 3 by diamonds. The deviation from the data points of the homo-metal compounds is very small. It is reasonable by considering the discussions in the previous sub-section; L is determined mainly by the choice of the ligand and the counter anion, and l_1 is almost equal to the sum of the ion radii of Pt^{4+} and X^- ions.

2-3. Control of the Optical Gap Energies. We discuss here the interrelation between the optical gap energies and the amplitude of the halogen distortions. In the MX chain compounds, the lowest excitation corresponding to the optical gap is the CT exciton transition expressed as ($M^{2+}(d^8)$, $M^{4+}(d^6)\rightarrow M^{3+}(d^7)$, $M^{3+}(d^7)$).[6,20] In Table 1, the energies of the CT exciton transition (E_{CT}), that is, the optical gap energy evaluated from the polarized reflectivity spectra by using the Kramers–Kronig transformation are listed for the various MX chain compounds. In Fig. 5 (1), E_{CT} is plotted for the Pt compounds and the hetero-metal (Pt and Pd) compounds as a function of the distortion parameter d ($d = 2\Delta/L$). E_{CT} is mainly determined by the energy difference E_s between the M^{2+} site and the M^{4+} site shown in Fig. 2 (B). The linear relationship between E_{CT} and d corresponds to the fact that E_s is proportional to Δ. Therefore, we can control the magnitudes of E_{CT}, since we know how to change the values of Δ by the choice of the constituent elements, as detailed in Sect. 2-1.

The magnitudes of E_{CT} in the hetero-metal compounds are larger than those in the Pt compounds. This result can be interpreted by considering the site energy difference in the hetero-metal compounds. Roughly speaking, the difference between the two dotted lines in Fig. 5 (1) corresponds to the energy difference between the 4d orbitals of Pd^{2+} ions in the hetero-metal compounds and 5d orbitals of Pt^{2+} ions in the homo-metal compounds.

In Table 1, abbreviations of the MX chain compounds detailed in this paper are listed. In the following, we will use them instead of the rational formula for convenience. For [Pt(en)$_2$][Pt(en)$_2$Br$_2$](ClO$_4$)$_4$, two monoclinic polymorphisms, Pt–Br–Pt–I and Pt–Br–Pt–II have been obtained to date, which are characterized by the space group $P2_1/m$[60] and $C2/m$,[58] respectively. In these two compounds, conformations of

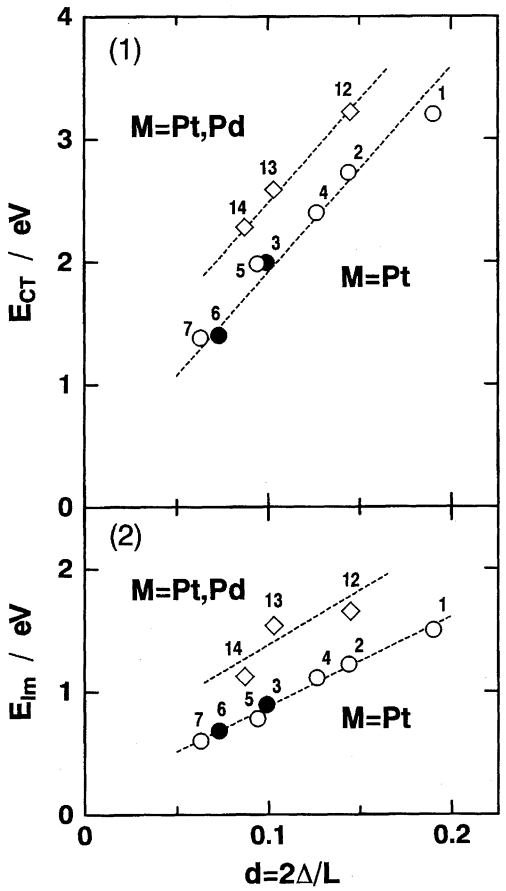

Fig. 5. The peak energies of the CT exciton absorption bands (E_{CT}) (1) and the STE luminescence bands (E_{Im}) (2) as a function of the distortion parameter d. The numbers in this figure correspond to those in Table 1. The data of the Pt compounds are represented by circles. The data of the hetero-metal compounds with M = Pt and Pd are represented by diamonds. The open and filled marks indicate the compounds with Y = ClO_4 and Y = halogen, respectively.

the (en) molecules are slightly different from each other, resulting in the difference of L, $d(\Delta)$, and E_{CT}.

3. Relaxation Process of the Photoexcited States Related with Solitons, Polarons, and Excitons

Photogeneration and relaxation processes of solitons, polarons, and excitons in the MX chain compounds are strongly dependent on the optical gap energies E_{CT}, that is, the degree of electron lattice interaction. In the Subsection 3-1, we review how the luminescence process from STE depends on E_{CT}. In Sect. 3-2, we will report the characterization of the photoinduced gap states in the MX chain compounds having the relatively large E_{CT}, by comparing the results of PA and PESR measurements on the homo-metal compound, Pt–Br–Pt–II, with those on the hetero-metal compound, Pt–Br–Pd.[37] In Sect. 3-3, we discuss the relaxation dynamics of the photoexcited states from the excitation profiles of the gap states and the STE luminescence, and the time characteristics of the STE luminescence.[37] Especially, the conversion of excitons to spin-soliton pairs will be elucidated. In Sect. 3-4, we will report the characterization of the photoinduced gap states in the MX chain compounds having small E_{CT}.[21,25] Moreover, the general relaxation process of the photoexcited states which involve solitons, polarons, and excitons is discussed.

3-1. Self-Trapped Exciton (STE) Luminescence. In the MX chain compounds, the luminescence from the self-trapped exciton (STE) with a large Stokes shift is observed.[3—6,20] In the 1-D system, there is no potential barrier between a free exciton and an STE,[72] so that an optically excited exciton will immediately induce a local lattice distortion and relax to a metastable state such as an STE. The energies of the luminescence (E_{lm}) are listed in Table 1 and plotted against the distortion parameter d in Fig. 5 (2). E_{lm} is 40—50% of E_{CT} for the Pt compounds and 50—60% of E_{CT} for the hetero-metal compounds (Pt–X–Pd) in common. Such a large Stokes shift comes from the large lattice relaxation energy of the STE due to the dissolution of the halogen distortions.

The efficiency of the luminescence process considerably changes by a decrease in the gap energies. In Fig. 6, the relative intensities of luminescence for the 2.4 eV excitation measured at 2 K are plotted. There are two significant features in Fig. 6; first, the intensity of luminescence decreases by more than four orders of magnitude when E_{CT} decreases from 2.7 to 1.4 eV. This result suggests that with decrease of the halogen distortions, the STE becomes rather unstable. Second, the intensities of luminescence in the hetero-metal compounds (Pt–X–Pd) and the Pt compounds with the 2-D ordered CDW (2-D Pt–X–Pt) are relatively larger than those of the Pt compounds with 1-D CDW (Pt–X–Pt). We will discuss these characteristic features more in detail in Sect. 3-3.

3-2. Photogeneration of Solitons and Polarons in the MX Chain Compounds with Large Gap Energies. Figure 7 (1) shows the PA spectrum $\Delta\alpha$ [photoinduced change of $\alpha = kd$] of a Pt–Br–Pt–II single crystal with the excitation

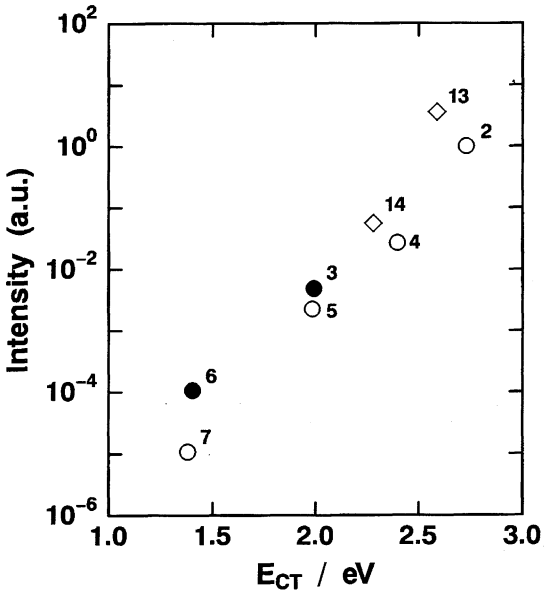

Fig. 6. The normalized integrated intensity of the luminescence as a function of E_{CT} in the MX chain compounds. The numbers in this figure correspond to those in Table 1. Luminescence is measured at 2 K with the excitation of 2.4 eV. The data of the Pt compounds are represented by circles. The data of the heterometal compounds with M = Pt and Pd are represented by diamonds. The open and filled marks indicate the compounds with Y = ClO_4 and Y = halogen, respectively.

of 3.2 eV at 77 K. Here, k and d are the absorption coefficient and the sample thickness, respectively. In the measurement, polarization of both the irradiation light (E_{ex}) and the transmission light (E) is taken parallel to the chain axis b. In Fig. 7 (1), the polarized absorption spectrum for $E//b$ at 77 K is also presented by the dotted line. The arrow indicates the optical gap energy E_{CT}. The PA signal was characteristic only for $E//b$ and no PA signal could be detected for $E\perp b$. A midgap absorption band labeled as α at 1.55 eV and a weak shoulder structure labeled as β at 1.79 eV are observed in as-grown samples, which are enhanced by light irradiation. In addition, a very weak PA band labeled as γ has been observed at the lower energy side. To discriminate the observed PA bands, we measured the time characteristic of the normalized peak intensities of the three structures; these results are shown in Fig. 7 (2). The band γ decays in a different manner compared with the bands α and β, suggesting that optically excited states include two different photoproducts associated with α, β, and the lower energy band γ.

In Pt–Br–Pd, spectral shapes of PA signals are considerably changed. As shown in Fig. 8 (1), there is no prominent structure in the absorption spectrum below the optical gap energy E_{CT}, while two PA bands are observed with the 3.2 eV excitation, which are labeled as $\mathbf{a}_1$ and $\mathbf{a}_2$. Time dependence of these PA bands is presented in Fig. 8 (2). They show the same time characteristics, suggesting that they are related to the same excited state.

To investigate the generation process of the photoproducts, we measured excitation profiles of the PA bands (α and γ

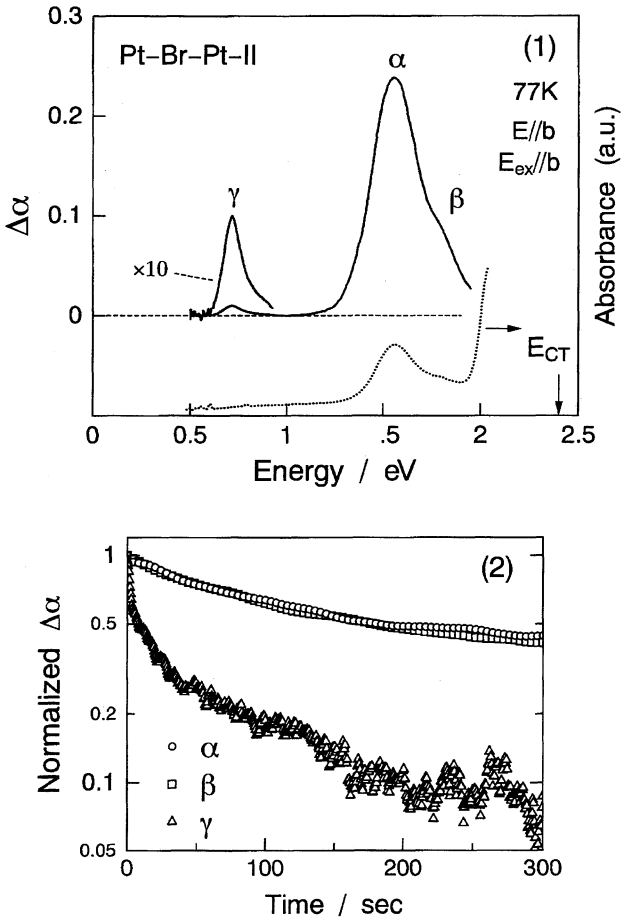

Fig. 7. (1) PA spectrum with the excitation of 3.2 eV (5 mW cm^{-2}) and polarized absorption spectrum (dotted line) measured at 77 K in Pt–Br–Pt–II. Both the excitation lights (E_{ex}) and the transmission lights (E) are polarized parallel to the b axis. (2) Time-dependence of the normalized peak intensities of the PA bands with excitation of 3.2 eV (22 mW cm^{-2}) at 77 K.

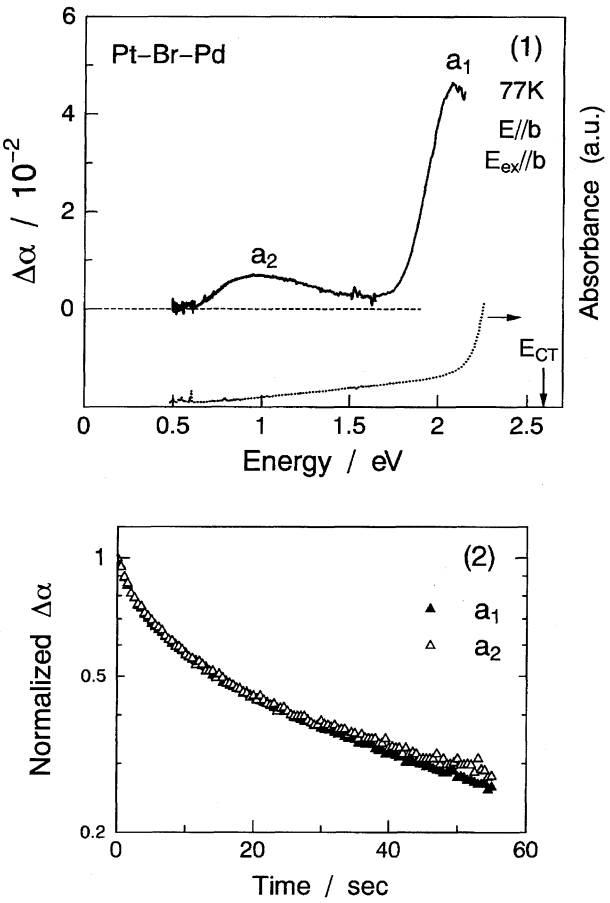

Fig. 8. (1) PA spectrum with the excitation of 3.2 eV (20 mW cm^{-2}) and polarized absorption spectrum (dotted line) measured at 77 K in Pt–Br–Pd. Both the excitation lights (E_{ex}) and the transmission lights (E) are polarized parallel to the b axis. (2) Time-dependence of the normalized peak intensities of the PA bands with the excitation of 3.2 eV (20 mW cm^{-2}) at 77 K.

in Pt–Br–Pt–II, and $\mathbf{a}_1$ in Pt–Br–Pd). Intensities of these PA bands I_{PA} are almost proportional to the square root of excitation density I, suggesting that they decay by the bimolecular recombination process.[73,74] So that, the excitation profiles of the PA signals are evaluated by taking into account the relation $I_{PA} \propto I^{0.5}$. The results are shown in Fig. 9 by the circles for band α, the triangles for band γ in Pt–Br–Pt–II,[75] and the inverted triangles for band $\mathbf{a}_1$ in Pt–Br–Pd. The dotted line is the absorption spectra (ε_2) due to the charge transfer (CT) excitons, mentioned in the previous section. As seen in Fig. 9, the CT exciton does not contribute to generation of the band γ, but to the band α. The band γ is photogenerated only for the excitation energies higher than E_{CT}. The excitation profile of the band $\mathbf{a}_1$ in Pt–Br–Pd is quite similar to that of the band γ in Pt–Br–Pt–II.

To clarify whether the photoproducts have spins ($s = 1/2$) or not, we studied ESR and PESR. Figure 10 (1) A shows the ESR signal in an as-grown single crystal of Pt–Br–Pt–II for the magnetic field $H \perp b$ measured at 4 K. Concentration of spin is ca. 10^{-4} per Pt site. Figure 10 (1) B–D show the photoinduced changes of ESR signals (the difference spectra) for the typical excitation energies: 1.8, 2.5, and 3.1 eV. At 4 K, life times of the observed photoinduced ESR signals are extremely long, so that excitation lights with very low power (ca. 1.5×10^{15} photon cm^{-2} s^{-1}) are used for every excitation to avoid saturation effects. Excitation energy dependence of the intensity of the PESR signals is shown by the rectangles in Fig. 9. The ESR signal does not change due to the excitation of 1.8 eV, which is enhanced by the 2.5 eV excitation. The 2.5 eV excitation does not generate the band γ, but enhances the bands α and β. Namely, the photoinduced ESR signals should be related to the bands α and β. In the present studies, we cannot determine whether the band γ is related to a spin ($s = 1/2$) or not. The intensity of the band α is about 50 times larger than that of the band γ, as seen in Fig. 7. So that, even if the excited state responsible for the band γ has a spin, its PESR signals will not be discriminated from the large PESR signals related to the band α and β. We performed similar measurements for Pt–Br–Pd. As seen in Fig. 10 (2) A, there is no structure in an as-grown sample. PESR signal is observed only by the excitation above 2.7 eV. Such a

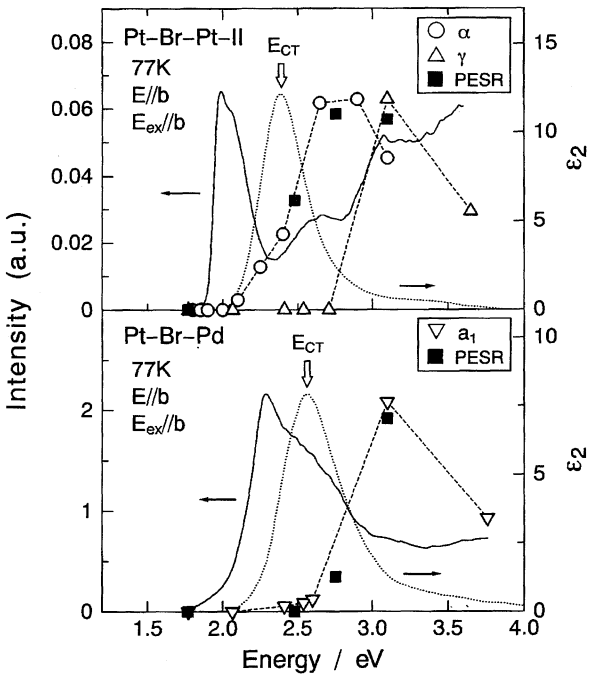

Fig. 9. Excitation profiles for the intensities of the PA (○: the band α: and △: the band γ in Pt–Br–Pt–II, and ▽: the band $\mathbf{a}_1$ in Pt–Br–Pd), PESR (■) and luminescence (solid lines) at 77 K and the imaginary parts of the dielectric constants ε_2 (broken lines) at room temperature.

behavior is in agreement with the excitation profile of the PA band γ. Namely, the band γ is associated with a spin ($s = 1/2$).

Here, we will discuss the origin of the observed PA and PESR signals. They are probably due to the gap states such as solitons and polarons.[76—78] Figure 11 shows the localized energy levels of polaron (P^- and P^+), spin-soliton (S^0) and charged-soliton (S^- and S^+) in the case that the transfer energy T between the neighboring metal ions is equal to zero.[78] The more realistic electronic structures of these gap states with a large T are presented schematically in Fig. 12. Several groups have reported theoretically the absorption spectra of the gap states in the 1-D Peierls–Hubbard model.[41—44,46] Their spectral features are essentially the same; two absorption bands arise for a polaron, and one midgap band for either a spin- or charged-soliton. In Fig. 12, the solid arrows indicate the possible optical transitions. For a polaron, it has been demonstrated that the oscillator strengths of the transitions indicated by the dashed arrows are extremely weak and only the two transitions indicated by the solid arrows are possible.

From the time-dependence shown in Fig. 8 (2), we can conclude that the PA bands $\mathbf{a}_1$ and $\mathbf{a}_2$ of Pt–Br–Pd largely split in the intragap region have the same origin. Such a doublet structure is characteristic to the absorption of polarons. The gap states responsible for these bands have spin $s = 1/2$ as demonstrated from the PESR measurements, so that they can

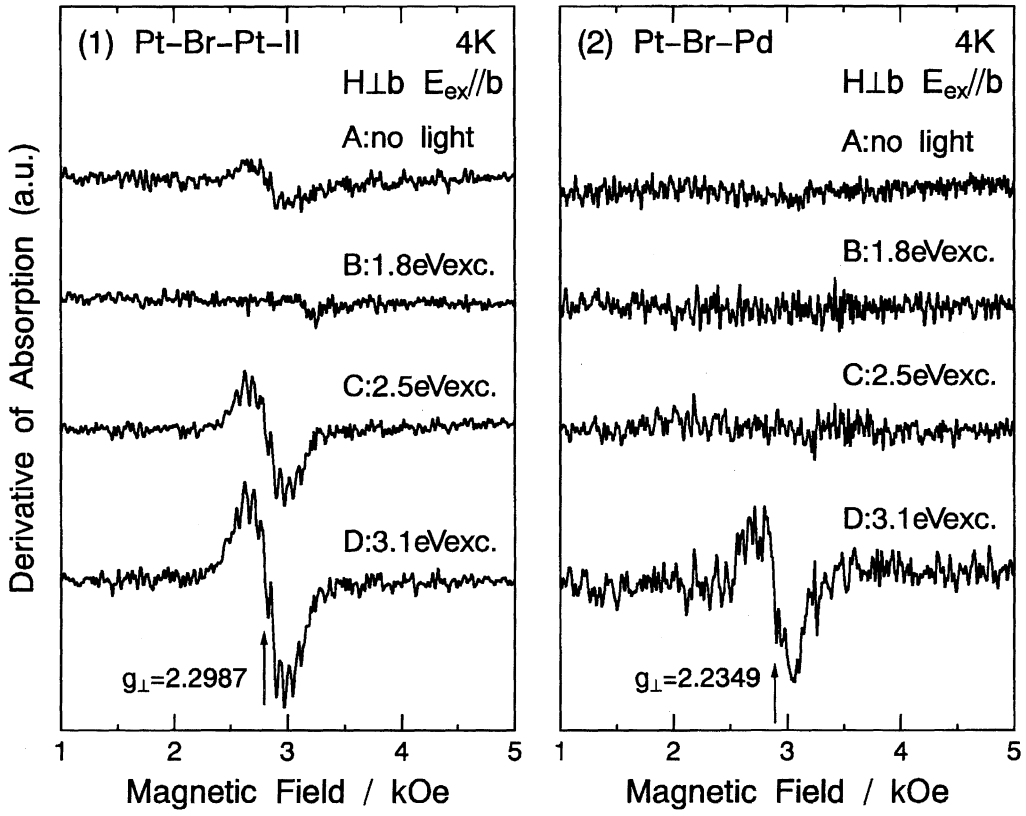

Fig. 10. ESR signals in as-grown single crystal (A) and photoinduced change of ESR signals (B–D) for Pt–Br–Pt–II (1) and Pt–Br–Pd (2) at 4 K. The intensity of the excitation lights is 1.5×10^{15} photon cm^{-2} s^{-1}. The excitation lights are polarized parallel to the b axis.

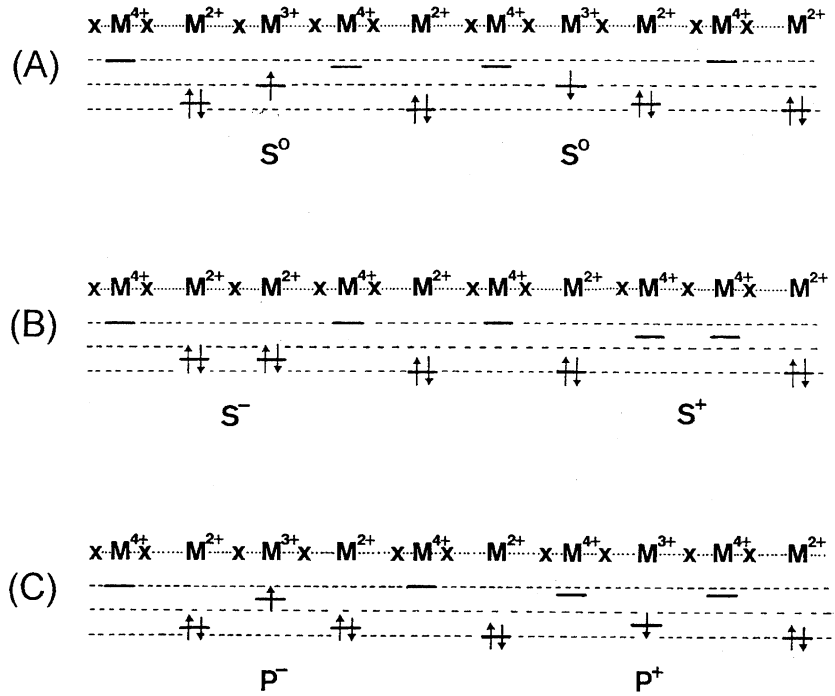

Fig. 11. Localized energy levels: (A) spin-solitons (S^0), (B) charged-soliton (S^-, S^+), and (C) polarons (P^-, P^+).

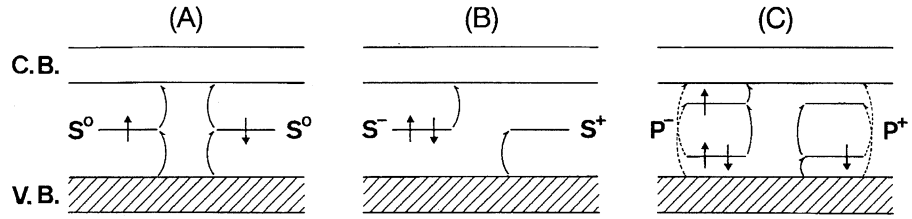

Fig. 12. Schematic electronic structures: (A) spin-solitons (S^0), (B) charged-solitons (S^-, S^+), and (C) polarons (P^-, P^+).

be attributed to polarons.

In Pt–Br–Pt–II, the time characteristics of the bands α, β are different from that of the band γ, so that they cannot be attributed to the same excited state. The important point is that midgap bands α and β are not detected in Pt–Br–Pd. Pt–Br–Pd has the nondegenerate ground state, so that solitons should not be stabilized. Therefore, it is natural that the bands α and β are attributed to solitons. From the PESR studies, the bands α and β are associated with a spin, so that solitons responsible for α and β, are spin-solitons, since charged-solitons have no spin.

Next, we will discuss the possible interpretations for the band γ in Pt–Br–Pt–II. The energy of the band γ is small, about $0.3\times E_{CT}$. Considering such a small energy, we can attribute the band γ to the lower energy transition of polarons, which corresponds to the $\mathbf{a}_2$ band in Pt–Br–Pd. The lower energy transitions of polarons are observed around $0.37\times E_{CT}$ in Pr–Br–Pd, and $0.33\times E_{CT}$ in Pt–I–Pt and $0.35\times E_{CT}$ in 2-D Pt–Br–Pt, as reported in the next subsection. Moreover, the excitation profile of polarons (the band $\mathbf{a}_1$) in Pt–Br–Pd is quite similar to that of the band γ, as shown in Fig. 9. This result also supports the assignment of the band γ to the lower energy transition of polarons. As seen in Fig. 7 (1) and Fig. 8 (1), the band $\mathbf{a}_2$ of Pt–Br–Pd is considerably broadened as compared with the band γ of Pt–Br–Pt–II. As for the polarons in Pt–Br–Pd, we should consider the electron-hole asymmetry. In Pt–Br–Pd, electron polarons exist on the Pt

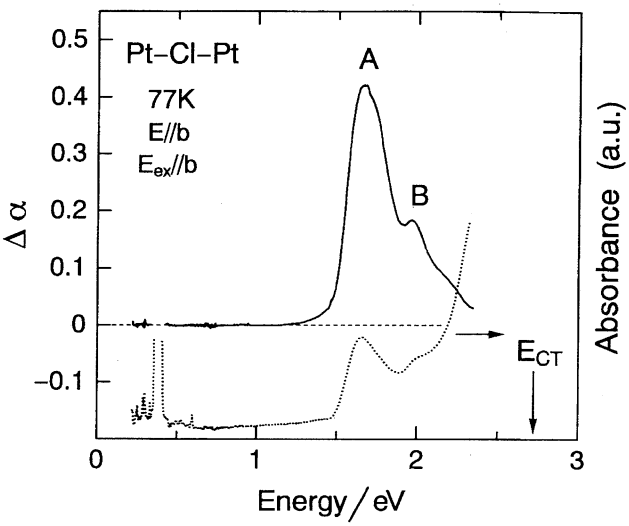

Fig. 13. PA spectrum of Pt–Cl–Pt with the excitation of 2.4 eV (5 mW cm^{-2}) and polarized absorption spectrum (dotted line) measured at 77 K.

sites and hole polarons on the Pd sites. Therefore, the PA energies for a positively-charged polaron and a negatively-charged one will be slightly different from each other due to the difference in the magnitude of U on the metal ions. The broad $\mathbf{a}_2$ band might be composed of the two transitions slightly split due to the electron-hole asymmetry.

It is worthwhile comparing the photoinduced studies on Pt–Br–Pt–II presented here with those on $[Pt(en)_2][Pt(en)_2Cl_2](ClO_4)_4$ (Pt–Cl–Pt), in which the detailed studies about photogenerations of solitons and polarons have been reported.[9,14,27,79—82] Figure 13 shows the PA spectrum of Pt–Cl–Pt, which is in agreement with that previously reported.[9] The PA bands named as A and B have been observed in the PA spectrum. There has been a long controversy about whether they are due to polarons[9,14] or spin-solitons.[8,16,27] Spectral features of the PA bands A and B in Pt–Cl–Pt are quite similar to those of the α and β bands observed in Pt–Br–Pt–II. Therefore, we consider that the A and B bands would also be attributed to spin-solitons. In Pt–Cl–Pt, the photoinduced ESR signal associated with the PA bands A and B, has also been observed.[79—82] This signal is composed five hyperfine structures with an splitting of 176 Gauss, which are accompanied by the super-hyperfine structures with an splitting of 16 Gauss. The detailed analysis of these structures given by N. Kuroda et al. supports that the PESR signals are due to spin-solitons.[80—82] In Pt–Br–Pt–II, number of hyperfine structures increases to be 10 and the splitting is ca. 71 Gauss as seen in Fig. 10 (1). Such values suggest delocalization of a spin over many metal and bridging halogen ions in Pt–Br–Pt–II as compared with the case in Pt–Cl–Pt. Such a delocalization of a spin may be interpreted from the fact that the Pt–X transfer energy is larger for X = Br than for X = Cl.

Here, we will comment on the spectral features of the PA bands α and β due to spin-solitons. As shown in Fig. 12, a most simple model expects that a single absorption band will arise at half of the gap energy ($1/2E_{CT}$) for spin-solitons. However, in the PA spectrum experimentally obtained, the absorption of spin-solitons in Pt–Br–Pt–II is composed of the two bands α and β, and the energies of these bands exceed $1/2E_{CT}$. The theoretical study given by K. Iwano and K. Nasu indicates that the absorption spectrum of a spin-soliton show a doublet structure in the presence of lattice fluctuations.[42] This might explain the existence of the two PA bands α and β for spin-solitons. K. Iwano has also reported that the transition energy for spin-soliton strongly depends on the magnitude of the on-site Coulomb energy U.[47] With increase of U, the absorption energy of a spin-soliton increases.[47] Using reasonable values of U, the electron-lattice interaction S, the nearest neighbor Coulomb energy V, and the transfer energy T, 0.6 E_{CT} has been obtained for the absorption of a spin-soliton.[47] This value is close to the observed energy of the band α (ca. 0.65 E_{CT}) in Pt–Br–Pt–II. In *trans*-$(CH)_x$, an absorption due to spin-solitons also locates at the energy (ca. 1.35 eV) considerably larger than the half of the gap energy (ca. 0.7 eV),[83] because of the large on-site Coulomb energy U.[84]

3-3. Conversion of the Excitons to the Solitonic States. In this subsection, we will discuss the relaxation dynamics of the photoexcited states. It is interesting to clarify the interrelation between the luminescence process from STE and the dissociation process to soliton or polaron pairs followed by nonradiative recombinations. In order to study such a competition in detail, we will compare the excitation profiles of the STE luminescence with those of the PA signals for the two compounds, Pt–Br–Pt–II and Pt–Br–Pd. In Pt–Br–Pt–II, both of spin-solitons and polarons are photogenerated, while in Pt–Br–Pd, only polarons are possible. From the comparison of the two compounds, we expect to discriminate the contributions of solitonic state on the relaxation processes.

The excitation profiles of the STE luminescence at 77 K are shown by the solid lines in Fig. 9. In Pt–Br–Pt–II, the intensity of luminescence begins to increase from the band edge at about 1.9 eV and then decreases sharply around E_{CT}. When the excitation energy exceeds E_{CT}, the luminescence intensity increases again. In Pt–Br–Pd, the excitation profile of the STE luminescence is considerably different from that in Pt–Br–Pt–II. First, a sharp decrease of the luminescence intensity around E_{CT} observed in Pt–Br–Pt–II is not detected in Pt–Br–Pd. The luminescence intensity only gradually decreases with increase of the excitation energy in Pt–Br–Pd. Second, the relative intensity of luminescence in Pt–Br–Pd is larger by at least one order than that in Pt–Br–Pt–II in the whole energy region. Notice the right vertical scale of Fig. 9.

In Pt–Br–Pt–II, the sharp decrease of luminescence intensity around E_{CT} corresponds to the increase of the generation efficiency of spin-solitons (open circles in Fig. 9). It suggests that the generation process of spin-solitons competes with the luminescence process. Namely, conversions from excitons to spin-soliton pairs occur and they decay nonradiatively. This interpretation is supported from the fact that the luminescence intensity does not decrease for the excitations around E_{CT} in Pt–Br–Pd, in which solitons are not photogenerated. The difference of the relative intensity of luminescence between Pt–Br–Pt–II and Pt–Br–Pd suggests that most of the excitons in Pt–Br–Pt–II decay nonradiatively. The excitation profiles of polarons in the two compounds are essentially the same. Polarons are not generated from the CT excitons, but are generated only from the higher energy excited states, corresponding probably to the electron-hole continuum. In the high energy regions where the excitation energy exceeds 3 eV, the generation process of polarons might also compete with the luminescence process.

Next, we will discuss the dynamics of the exciton to soliton conversion. In the above discussion, it is difficult to deduce whether the solitonic states are generated directly from the free excitons or are generated from the STEs. In the latter case, the time-characteristics of the STE luminescence will be affected by the transition rate to the solitonic state. In Fig. 14, the time-integrated luminescence spectra due to STEs at 10 K are shown by solid lines. Typical results of luminescence decay are shown in the inset of Fig. 14 with the detection energies E_{det} of 1.19 eV for Pt–Br–Pt–II and 1.52 eV for Pt–Br–Pd. These time-characteristics of luminescence are

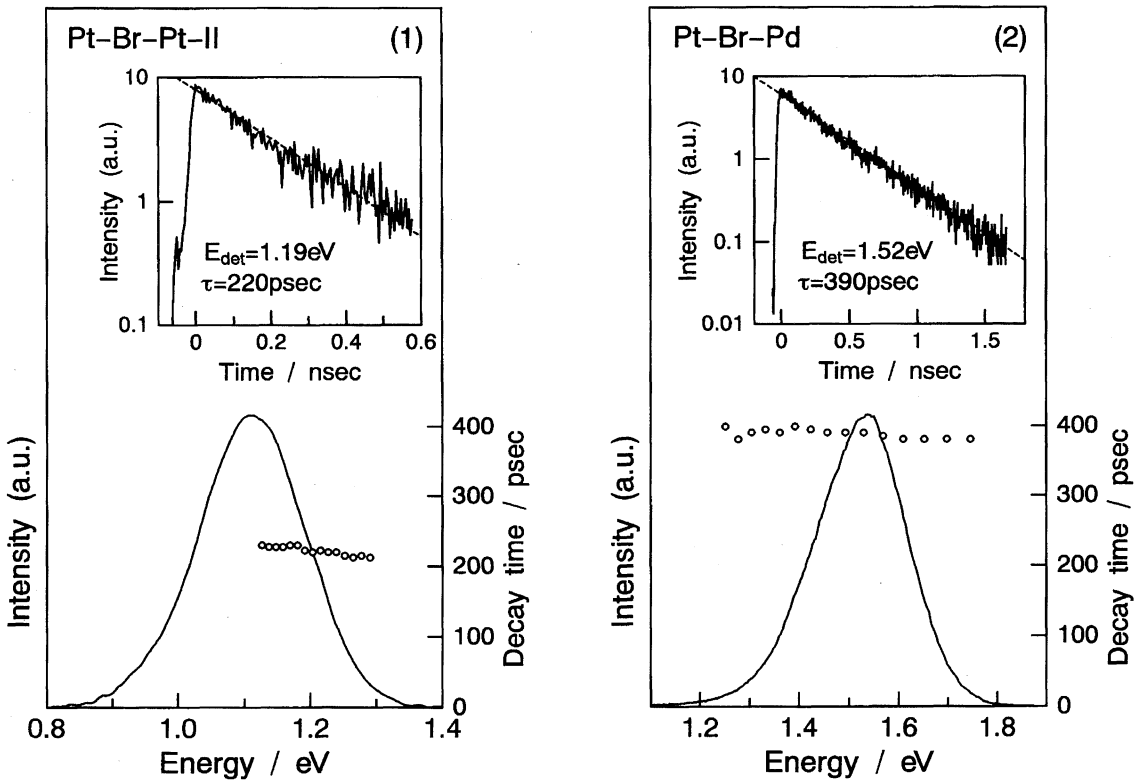

Fig. 14. Luminescence spectra (solid lines) and luminescence decay time τ (circles) at 10 K for the excitation energy of 3.2 eV in Pt–Br–Pt–II (1) and Pt–Br–Pd (2). Both the excitation lights (E_{ex}) and the emission lights (E) are polarized parallel to the b axis. Insets are the time characteristics of the luminescence at 10 K for the detection energies of 1.19 eV in Pt–Br–Pt–II and 1.52 eV in Pt–Br–Pd.

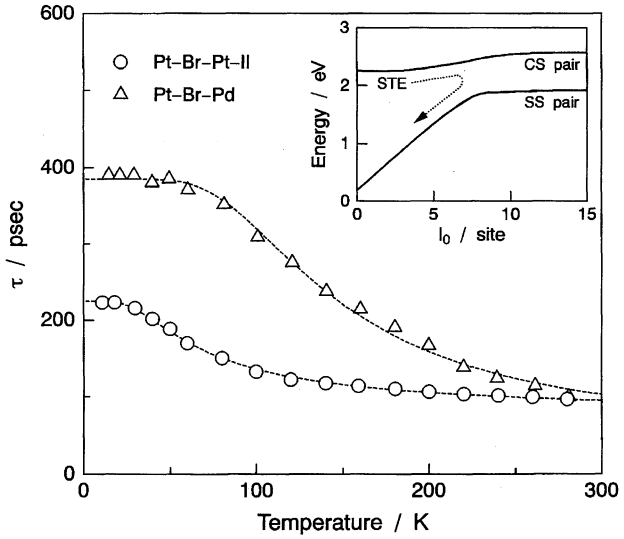

Fig. 15. Temperature dependence of the luminescence decay time τ. The detection energies are 1.19 eV in Pt–Br–Pt–II and 1.52 eV in Pt–Br–Pd. The inset shows the cross section of the potential energy surfaces reported by Iwano (taken from Ref. 47).

almost reproduced by the single exponential decay. For these detection energies, decay times τ are 220 ps in Pt–Br–Pt–II and 390 ps in Pt–Br–Pd. In Fig. 14, the E_{det} dependence of τ is plotted by the open circles. τ is almost independent of E_{det} within the luminescence band.

The radiative life time τ_r of the STE has been previously evaluated from the oscillator strength of the CT exciton transition, which is 4—6 ns in Pt–X–Pt and Pt–Br–Pd compounds.[11,32] The observed decay time of luminescence is at least one order of magnitude smaller than τ_r. Therefore, annihilations of the STEs should be dominated by nonradiative processes. To obtain more detailed information about nonradiative processes, the temperature dependence of the time characteristics of luminescence was measured. In Fig. 15, the decay time τ is plotted as a function of temperature for the detection energy of 1.19 eV in Pt–Br–Pt–II (circles) and 1.52 eV in Pt–Br–Pd (triangles). Below the critical temperature T_c (20 K in Pt–Br–Pt–II and 50 K in Pt–Br–Pd), the decay time τ is almost unchanged. Above T_c, τ decreases gradually with increase of temperature. Such behavior of τ is similar to that previously reported in Pt–Cl–Pt.[32] Here, we will adopt the following simple formula to explain the temperature dependence of τ:

$$\tau = [\tau_0^{-1} + \tau_a^{-1}\exp(-\Delta/kT)]^{-1}. \quad (1)$$

In this formula, the first and second terms show the temperature-independent decay rate and the thermal-activation-type decay rate, respectively. The obtained temperature dependence of τ is well reproduced by this formula, as shown by the broken lines in Fig. 15. The used parameter values are $\tau_0 = 255$ ps, $\tau_a = 115$ ps, and $\Delta = 9.5$ meV for Pt–Br–Pt–II, and $\tau_0 = 385$ ps, $\tau_a = 38$ ps, and $\Delta = 34$ meV for Pt–Br–Pd.

These temperature-dependent behaviors of τ are independent of samples in both compounds, so that the nonradiative annihilation processes of the STEs are attributable to intrinsic origin. It is natural to consider that the difference in τ (or the parameter values Δ, τ_0, and τ_a) of the two complexes is related to the difference in the relaxation process to the solitonic states. τ of Pt–Br–Pt–II is smaller than that of Pt–Br–Pd in the whole temperature region. It is attributable to the fact that the conversion of the STE to the solitonic state can occur more easily in Pt–Br–Pt–II than in Pt–Br–Pd. Namely, the nonradiative decay of excitons deduced from the excitation profiles of luminescence in Pt–Br–Pt–II seems to occur by way of the conversion from the STE to the solitonic state.

Here, we will try to interpret our experimental results by referring to some theoretical expectations. Several authors reported the theoretical studies of the relaxation processes in the MX chain compound.[39,40,47] According to them, there is only a small barrier between the STE and the solitonic state, while a large barrier exists between the STE and the polaronic state. The recent calculation by Iwano based upon the extended Peierls–Hubbard model using reasonable parameters of T, S, U, and V has provided detailed potential energy surfaces.[47] In his calculation, the pattern of lattice deformation is assumed as follows

$$Q_l = (-1)^l Q_0[1 + \Delta Q(\tanh \theta(|\, l\,| - l_0/2) - 1)]. \quad (2)$$

Here, ΔQ, l_0, and θ are the depth of the deformation, the soliton-antisoliton distance, and the width of a soliton or STE, respectively. In the inset of Fig. 15, we present the cross sections of the first and second lowest potential surfaces at $\Delta Q = 1$ reported by Iwano (Fig. 9 in Ref. 47). The higher surface includes the STE and charged-soliton (CS) pair. The lower surface includes the spin-soliton (SS) pair and is connected to the ground state. They were calculated by selecting the parameter values for the homo-metal compound with E_{CT} of 2.6 eV. As E_{CT} of Pt–Br–Pt–II (2.4 eV) is close to that, this theoretical result can apply qualitatively to Pt–Br–Pt–II. As seen, the formation energy of a spin-soliton pair is smaller than that of a charge-soliton pair. According to Ref. 47, a transition from the STE to the spin-solitonic state is possible with the help of asymmetric vibrations. These expectations are in good agreement with our experimental results. In Pt–Br–Pt–II, it is reasonable to consider that Δ is a potential barrier between the STE and the solitonic state and τ_0^{-1} is a tunneling rate through the barrier. We can imagine the existence of the barrier in the inset of Fig. 15, when the transition from the STE to the solitonic state occurs at the large values of l_0. That is, the transition probability as a function of l_0 will determine the magnitude of the effective barrier height. In Pt–Br–Pt–II, the photogeneration efficiency of dissociated spin-solitons has been evaluated to be less than 10^{-3},[85] so that it is reasonable to consider that the main relaxation path of the STE will be the nonradiative geminate recombination process through the solitonic state indicated by the arrows in the inset of Fig. 15. Temperature dependence of τ in Pt–Br–Pd and that in Pt–Br–Pt–II can be explained by the same formula (Eq. 1) except for the difference in the values of parameters (Δ, τ_0, and τ_a). Therefore, a similar process is considered to dominate the nonradiative decay of STE in Pt–Br–Pd. In Pt–Br–Pd, with increase of l_0, the formation energy of a soliton pair will increase sharply, so that a soliton pair cannot be dissociated. This is the reason why solitons have never been observed in Pt–Br–Pd. Namely, the energy of potential surfaces presented in the inset of Fig. 15 should increase sharply with increase of l_0 in Pt–Br–Pd. In this case, the depth of the potential well around the STE increases. As a result, Δ will be enhanced and τ_0^{-1} will be decreased in Pt–Br–Pd as compared with those in Pt–Br–Pt–II. In these interpretations, τ_a^{-1} is related to the frequency of the motion in the potential well around the STE, that is, the frequency of the breathing mode of a charged-soliton pair. The enhancement of τ_a^{-1} in Pt–Br–Pd is reasonable, since the frequency of motion should increase with increase of the slope of the potential well.

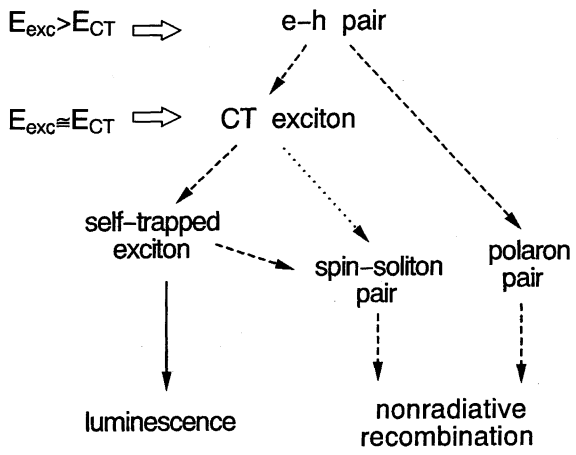

Fig. 16. Schematic diagram of the relaxation process of the photoexcited state in Pt–Br–Pt–II.

In Fig. 16, the relaxation processes of the photoexcited states in Pt–Br–Pt–II deduced from the results given above are schematically illustrated. From the higher energy excited states corresponding to the electron-hole continuum, polarons are generated. The CT excitons are relaxed to the STEs. A part of the STEs decay by luminescence, and the other parts are relaxed to the spin-solitonic states and then decay nonradiatively. The CT exciton with a large excess energy seems to dissociate into the spin-soliton pair before stabilizing as the STE, since the generation efficiency of the spin-solitons increases with increase of the excitation energy around E_{CT} as seen in Fig. 9. This process is shown by the dotted line in Fig. 16.

In *trans*-$(CH)_x$, photogeneration of spin-solitons has been extensively studied from the experimental and theoretical points of view. In *trans*-$(CH)_x$, a conversion of an electron-hole pair (the singlet B_u state) to a spin-soliton pair is essentially forbidden within the non-interacting electron model, due to the charge configuration symmetry in the bond ordered wave (BOW) ground state.[86,87] Additional interactions (i.e., a second nearest-neighbor hopping[86]) which break the charge configuration symmetry permit the photogeneration

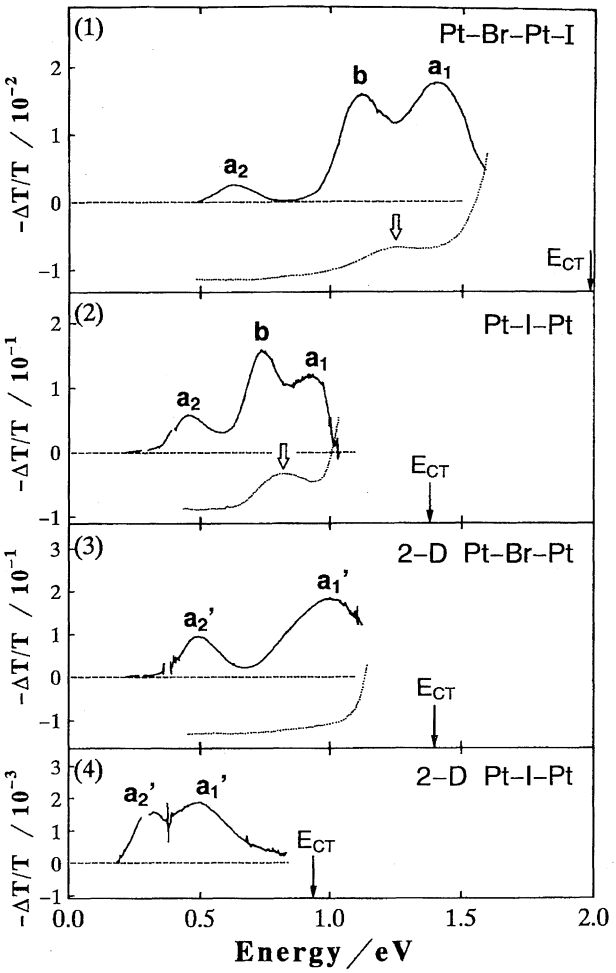

Fig. 17. PA spactra at 77 K for single crystals of Pt–Br–Pt–I, Pt–I–Pt, 2-D Pt–Br–Pt, and powder sample of 2-D Pt–I–Pt at 77 K. The excitation light is 2.4 eV (5 mW cm^{-2} for the single crystal samples and 100 mW cm^{-2} for the powder samples). Polarized absorption spectra along the *b* axis at 77 K are shown by the dotted lines.

of spin-solitons, as experimentally observed. On the other hand, the MX chain compounds are not charge configuration symmetric from the nature of CDW, so that photogeneration of spin-solitons is possible. Moreover, in contrast with *trans*-$(CH)_x$ in which the excitonic effect is considered to be not so large, the excitonic effect is rather important in the MX chain compounds. From these facts, the generation process of spin-solitons from the photoexcited states in the MX chain compounds is essentially different from that in *trans*-$(CH)_x$.

3-4. Photogeneration of Solitons and Polarons in the MX Compounds with Small Gap Energies. In this subsection, we will discuss the photogeneration of solitons and polarons in the MX chain compounds having relatively small gap energies E_{CT} ($E_{CT} < 2$ eV).[21,25] The PA spectra of Pt–Br–Pt–I, Pt–I–Pt, 2-D Pt–Br–Pt and 2-D Pt–I–Pt at 77 K are presented by the solid lines in Fig. 17. The PA measurements are performed on single crystals for the former three compounds, and on powder samples dispersed in KI pellet for the 2-D Pt–I–Pt compound. In Fig. 17, the polarized absorption spectra (dotted lines) for *E*//*b* at 77 K are also presented.

In Pt–Br–Pt–I and Pt–I–Pt, the PA signal shows a triplet structure, $\mathbf{a}_1$, $\mathbf{a}_2$, and **b**, while in 2-D Pt–X–Pt, the observed structure is a doublet, $\mathbf{a}_1'$ and $\mathbf{a}_2'$, and the mid-gap structure **b** does not exist. Time characteristics of each band have been also investigated.[21,25,31] The band **b** decays in a different manner compared with $\mathbf{a}_1$ and $\mathbf{a}_2$. The band $\mathbf{a}_1$ and $\mathbf{a}_2$ ($\mathbf{a}_1'$ and $\mathbf{a}_2'$) show the same decay characteristic. Namely, the optically excited states include two different types of photoproducts associated with the doublet $\mathbf{a}_1$, $\mathbf{a}_2$, and the mid-gap structure **b**.

Comparing the energy positions of the PA bands in Fig. 17 with the theoretical predictions in Fig. 12, it is natural to assign the doublet $\mathbf{a}_1$, $\mathbf{a}_2$ ($\mathbf{a}_1'$, $\mathbf{a}_2'$) to polarons and the **b** band to spin- or charged-solitons. These assignments are reasonable, taking account of the interchain interaction. Under the 2-D phase ordering of CDW, formation of a dissociated soliton pair requires a large scale of misalignment of CDW phases between the neighboring chains, which leads to excess energy. Namely, the degeneracy of a 1-D CDW state is excluded in 2-D Pt–X–Pt, similarly to Pt–Br–Pd. Accordingly, in 2-D Pt–X–Pt, soliton formation would be suppressed.

Next, we will discuss whether the origin of the **b** band is spin-solitons or charged-solitons. As for this, ESR measurements give important information. In the ESR measurements on as-grown samples of Pt–I–Pt and Pt–Br–Pt–I, a finite amount of paramagnetic spins (ca. 10^{-4} per site) was detected.[88] In the absorption spectrum of these two compounds, a weak absorption band was observed at nearly half of the gap energies, as indicated by the open arrows in Fig. 17. However, in 2-D Pt–Br–Pt, neither a defect-related absorption band nor paramagnetic spin has been detected. Taking account of the difference in the interchain interactions, we have attributed the weak absorption bands to spin-solitons confined by some crystal imperfections. Such defect-related absorption band and paramagnetic spin are also observed in Pt–Br–Pt–II as detailed in Sect. 3-2. Therefore, the absorption bands of Pt–I–Pt and Pt–Br–Pt–I indicated by the open arrows in Fig. 17 would be the same as the band α (β). However, the features of the photoinduced signals in Pt–I–Pt and Pt–Br–Pt–I are different from those in Pt–Br–Pt–II. In Pt–Br–Pt–II, the bands α, β observed in the as-grown samples are enhanced by light irradiations, while in Pt–I–Pt and Pt–Br–Pt–I the absorption bands are not enhanced by light irradiation. The energy of the PA band **b** is clearly different from that of the defect-induced absorption band. Considering the energy difference between the defect-induced absorption band and the PA band **b**, we conclude that the PA band **b** is attributable to charged-solitons. The energy difference between the absorption of spin-solitons and that of charged-solitons is probably due to the on-site Coulomb repulsion energy U, similarly to the case of *trans*-$(CH)_x$. In *trans*-$(CH)_x$, it has been found that the absorption energy of spin-solitons (ca. 1.35 eV) is considerably larger than that of charged-solitons (ca. 0.5 eV).[83]

As discussed in detail above, in Pt–Br–Pt–II having a large

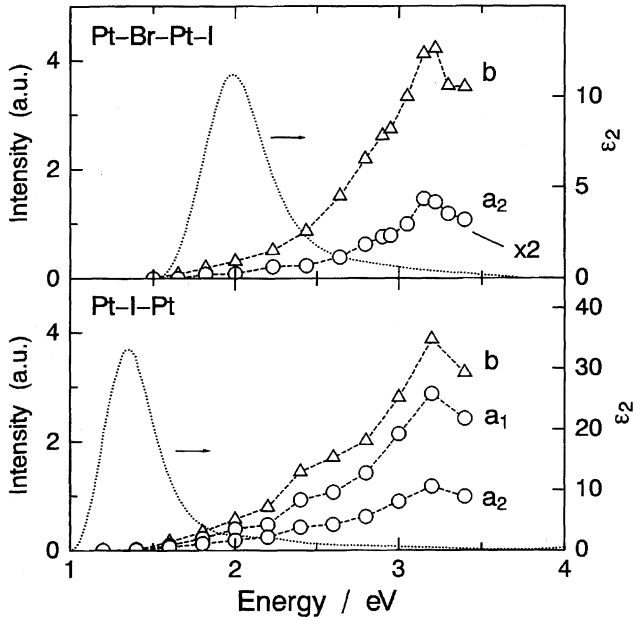

Fig. 18. Excitation profiles for the PA bands at 77 K in Pt–Br–Pt–I and Pt–I–Pt. The imaginary parts of the dielectric constants ε_2 at room temperature are shown by the broken lines.

gap ($E_{CT} > 2$ eV), spin-solitons are photogenerated, while in the compounds having the small gap ($E_{CT} < 2$ eV), charged-solitons are observed. Here, we will discuss the reason of the changes in the photogeneration of solitons. The formation energy of a charged-soliton is mainly determined by the on-site Coulomb repulsive energy U. With increase of T, the magnitudes of gap energies (E_{CT}) decrease. Simultaneously the effect of U will be suppressed, so that the formation energy of charged-solitons will decrease relatively to that of spin-solitons. This may be a reason why the charged-solitons are observed in the small gap compounds and the spin-solitons in the large gap compounds.

To obtain information about the generation process of the gap states, we measured the excitation profiles of the PA signals (I_{PA}) on Pt–Br–Pt–I and Pt–I–Pt, which are plotted in Fig. 18 together with the absorption spectra (ε_2) due to the CT excitons. Since it has been ascertained that the annihilation process of the observed gap states could be explained by the bimolecular recombination model,[21,25,34] the values of I_{PA} were normalized by using the relation $I_{PA} \propto I^{0.5}$ (I: the excitation density).[75] As seen, the CT exciton does not contribute to generation of polarons and charged-solitons, which are photogenerated only from the higher energy excited states. Such a feature is the same as that observed for polarons in Pt–Br–Pt–II and Pt–Br–Pd. The important point is that the excitation profiles of the charged-solitons in Pt–Br–Pt–I and Pt–I–Pt are different from those of the spin-solitons in Pt–Br–Pt–II. In the latter compound, the spin-solitons are photogenerated from the CT excitons, as demonstrated in Sect. 3-3.

As discussed in Sect. 3-1, the intensity of the STE luminescence decreases remarkably with the decrease of E_{CT}. The efficiency of the STE luminescence in Pt–I–Pt (Pt–Br–Pt–I) is about 10^{-3} (10^{-1}) times as small as that in Pt–Br–Pt–II, as shown in Fig. 6. This result suggests that the STE becomes unstable with decrease of E_{CT}. From these results and the excitation profiles of the gap states, the relaxation process of the photoexcited states in Pt–I–Pt and Pt–Br–Pt–I is interpreted as follows. The CT excitons will be relaxed to the STEs, and most of the STEs recombine nonradiatively. The barrier between the STE and the solitonic state connecting to the ground states will be very small, since the radiative decay process of the STEs is quenched. In this sense, such a relaxed state of the exciton could not be called as an "STE". On the other hand, a finite barrier will still exist between the exciton and the charged-soliton pair as well as the spin-soliton pair, since these gap states can not be generated from the CT exciton as demonstrated from the excitation profiles of the gap states. Thus, potential energy surfaces in these compounds seem to be considerably different from those in Pt–Br–Pt–II. The difference might be related to the fact that in Pt–I–Pt and Pt–Br–Pt–I, the effect of the electron-lattice interaction S is relatively small as compared with Pt–Br–Pt–II.[20] In fact, it has been reported that the shape of potential energy surfaces strongly depends on the physical parameters (S, T, U, and V).[47]

Finally, we will comment on the photoconducting behavior in the MX chain compounds. It has been found that the photo-conductivity is enhanced in the compounds having small gap energies (e.g. Pt–I–Pt[89] and 2-D Pd–Br–Pd[90]). The photocurrent should be related to the gap states detected by the PA measurements. In fact, the excitation profile of the photo-conductivity along the b axis[89] in Pt–I–Pt is almost the same as the profiles of the charged-solitons and polarons shown in Fig. 18. Since the excitation profiles of two gap states are almost the same, we can not determine whether the dominant carrier is the charged-solitons or the polarons. The recent analysis of the time and temperature dependence of the PA signals in Pt–I–Pt has revealed that the mobility of a polaron is larger than that of a charged-soliton.[34] In addition, the activation energy of the photoconductivity is in accord with that of the mobility of a polaron.[34] Namely, the dynamics of polarons dominates the photoconducting properties in Pt–I–Pt.

4. Summary

We have reported the remarkable tunability of the CDW states in the MX chain compounds. By substituting the metals (M = Pt, Pd, and Ni), the bridging halogens (X = Cl, Br, and I), the ligand molecules and the counter anions surrounding the 1-D chains, the amplitude of CDW, the optical gap energy, and the degeneracy of CDW can be widely controlled.

On the basis of these controls, we have clarified the nature of photoexcited states. By comparing the results of PA, ESR, and PESR measurements in the degenerate CDW states with those in the non-degenerate CDW states, we clearly characterized the photoinduced gap states as solitons and polarons. In the compounds having relatively large gap energies, spin-

solitons and polarons are photogenerated. From the excitation profiles of the PA signals and the STE luminescence, it was demonstrated that the luminescence process strongly competes with the dissociation to spin-soliton pairs. An analysis of the temperature dependence of the luminescence decay time revealed that a conversion from STE to solitonic state occurs through a finite potential barrier, the magnitude of which depends on degeneracy of CDW. Such a conversion experimentally observed is qualitatively in agreement with the theoretical expectations based upon the Peierls–Hubbard model. In the compounds having small gap energy, photogeneration of charged-solitons and polarons are observed. In this case, the charge-solitons might be more stabilized as compared to spin-solitons. With decrease of E_{CT}, the intensity of the luminescence remarkably decreases, suggesting that the STE becomes unstable. This is probably due to the relaxation to the solitonic states. Since the charged-soliton pair could not be produced from the CT exciton, the STE would decay directly to the ground state through the non-radiative relaxation process accompanied by the solitonic lattice distortions.

This work has been created in collaboration with Y. Shimada (Tohoku Univ.), Y. Kaga (Tohoku Univ.), Prof. Y. Oka (Tohoku Univ.), Prof. T. Mitani (JAIST), and Prof. K. Toriumi (Himeji Institute of Technology). The author (H. O.) thanks Dr. K. Iwano (KEK) and Prof. K. Nasu (KEK) for many enlightening discussions, and Prof. Y. Iwasa (JAIST) for the helpful support with the photoinduced PESR measurements. This work has been partly supported by the Nissan Science Foundation and a Grant-in-Aid for Science Research from the Ministry of Education, Science, Sports and Culture.

References

1) W. P. Su, J. R. Schrieffer, and A. J. Heeger, *Phys. Rev. Lett.*, **42**, 1968 (1979), and *Phys. Rev.*, **B22**, 2099 (1980).
2) For a review, see: A. J. Heeger, S. Kivelson, and J. R. Schrieffer, *Rev. Mod. Phys.*, **60**, 781 (1988).
3) H. Tanino and K. Kobayashi, *J. Phys. Soc. Jpn.*, **52**, 1446 (1983).
4) M. Tanaka, S. Kurita, Y. Okada, T. Kojima, and Y. Yamada, *Chem. Phys.*, **96**, 343 (1985).
5) H. Tanino, N. Koshizuka, K. Kobayashi, M. Yamashita, and K. Hoh, *J. Phys. Soc. Jpn.*, **54**, 483 (1985).
6) Y. Wada, T. Mitani, M. Yamashita, and T. Koda, *J. Phys. Soc. Jpn.*, **54**, 3143 (1985).
7) N. Matsushita, N. Kojima, T. Ban, and I. Tsujikawa, *J. Phys. Soc. Jpn.*, **56**, 3808 (1987).
8) N. Kuroda, M. Sakai, Y. Nishina, M. Tanaka, and S. Kurita, *Phys. Rev. Lett.*, **58**, 2212 (1987).
9) S. Kurita, M. Haruki, and K. Miyagawa, *J. Phys. Soc. Jpn.*, **57**, 1789 (1988).
10) M. Haruki and S. Kurita, *Phys. Rev.*, **B39**, 5706 (1988).
11) Y. Wada, K. Era, and M. Yamashita, *Solid State Commun.*, **67**, 953 (1988).
12) H. Tanino, W. Ruhle, and K. Takahashi, *Phys. Rev.*, **B38**, 12716 (1988).
13) N. Matsushita, N. Kojima, N. Watanabe, and I. Tsujikawa, *Solid State Commun.*, **71**, 253 (1989).
14) R. J. Donohoe, S. A Ekberg, C. D. Tait, and B. I. Swanson, *Solid State Commun.*, **71**, 49 (1989).
15) Y. Wada, T. Mitani, K. Toriumi, and M. Yamashita, *J. Phys. Soc. Jpn.*, **58**, 3013 (1989).
16) M. Sakai, N. Kuroda, and Y. Nishina, *Phys. Rev.*, **B40**, 3066 (1989).
17) H. Okamoto, K. Toriumi, T. Mitani, and M. Yamashita, *Phys. Rev.*, **B42**, 10381 (1990).
18) Y. Wada and M. Yamashita, *Phys. Rev.*, **B42**, 7398 (1990).
19) Y. Iwasa, E. Funatsu, T. Hasegawa, T. Koda, and M. Yamashita, *Appl. Phys. Lett.*, **59**, 2219 (1991).
20) H. Okamoto, T. Mitani, K. Toriumi, and M. Yamashita, *Mater. Sci. Eng.*, **B13**, L9 (1992).
21) H. Okamoto, T. Mitani, K. Toriumi, and M. Yamashita, *Phys. Rev. Lett.*, **69**, 2248 (1992).
22) H. Okamoto, K. Toriumi, T. Mitani, and M. Yamashita, *Mol. Cryst. Liq. Cryst.*, **218**, 247 (1992).
23) R. J. Donohoe, L. A. Worl, C. A. Arrington, A. Bulou, and B. I. Swanson, *Phys. Rev.*, **B45**, 13185 (1992).
24) R. Ikeda, M. Iida, T. Asaji, and A. Ghosh, *Chem. Phys. Lett.*, **210**, 229 (1993).
25) H. Okamoto and T. Mitani, *Prog. Theor. Phys., Suppl.*, **113**, 191 (1993).
26) H. Okamoto, T. Mitani, K. Toriumi, and M. Yamashita, *Synth. Met.*, **55**, 524 (1993).
27) N. Kuroda, M. Ito, Y. Nishina, and M. Yamashita, *J. Phys. Soc. Jpn.*, **62**, 2237 (1993).
28) F. H. Long, S. P. Love, B. I. Swanson, and R. H. Mckenzie, *Phys. Rev. Lett.*, **71**, 762 (1993).
29) H. Ooi, M. Yamashita, and T. Kobayashi, *Solid State Commun.*, **86**, 789 (1993).
30) H. Ooi, M. Yoshizawa, M. Yamashita, and T. Kobayashi, *Chem. Phys. Lett.*, **210**, 237 (1993).
31) H. Okamoto, Y. Oka, T. Mitani, K. Toriumi, and M. Yamashita, *Mol. Cryst. Liq. Cryst.*, **256**, 161 (1994).
32) Y. Wada, U. Lemmer, E. O. Gobel, M. Yamashita, and K. Toriumi, *Phys. Rev.*, **B52**, 8276 (1995).
33) H. Okamoto, Y. Shimada, Y. Oka, A. Chainani, T. Mitani, K. Toriumi, K. Inoue, T. Manabe, and M. Yamashita, *Phys. Rev.*, **B54**, 8438 (1996).
34) H. Okamoto, Y. Oka, T. Mitani, and M. Yamashita, *Phys. Rev.*, **B55**, 6330 (1997).
35) H. Okamoto, in "Relaxations of Excited States and Photoinduced Structural Phase Transitions," ed by K. Nasu, Springer, New York (1997), p. 92.
36) N. Kuroda, Y. Wakabayashi, M. Nishida, N. Wakabayashi, M. Yamashita, and N. Matsushita, *Phys. Rev. Lett.*, **79**, 2510 (1997).
37) H. Okamoto, Y. Kaga, Y. Shimada, Y. Oka, Y. Iwasa, T. Mitani, and M. Yamashita, *Phys. Rev. Lett.*, **80**, 861 (1998).
38) K. Nasu, *J. Phys. Soc. Jpn.*, **52**, 3865 (1984).
39) A. Mishima and K. Nasu, *Phys. Rev.*, **B39**, 5758 (1989).
40) A. Mishima and K. Nasu, *Phys. Rev.*, **B39**, 5763 (1989).
41) Y. Tagawa and N. Suzuki, *J. Phys. Soc. Jpn.*, **59**, 4074 (1990).
42) K. Iwano and K. Nasu, *J. Phys. Soc. Jpn.*, **61**, 1380 (1992).
43) J. T. Gammel, A. Saxena, I. Batistic, A. R. Bishop, and S. R. Phillpot, *Phys. Rev.*, **B45**, 6408 (1992).
44) S. M. Webber-Milbrodt, J. T. Gammel, A. R. Bishop, and E. Y. Lor, Jr., *Phys. Rev.*, **B45**, 6435 (1992).
45) Y. Tagawa and N. Suzuki, *J. Phys. Soc. Jpn.*, **64**, 1800 (1995).

46) Y. Tagawa and N. Suzuki, *J. Phys. Soc. Jpn.*, **64**, 2212 (1995).
47) K. Iwano, *J. Phys. Soc. Jpn.*, **66**, 1088 (1997).
48) S. Kida, *Bull. Chem. Soc. Jpn.*, **38**, 1804 (1965).
49) K. P. Larsen and H. Toftlund, *Acta Chem. Scand., Ser. A*, **A31**, 182 (1977).
50) H. Toftlund, P. W. Jensen, and C. S. Jacobsen, *Chem. Phys. Lett.*, **142**, 286 (1987).
51) N. Matsumoto, M. Yamashita, and S. Kida, *Bull. Chem. Soc. Jpn.*, **51**, 2334 (1978).
52) H. Okamoto, K. Okaniwa, T. Mitani, K. Toriumi, and M. Yamashita, *Solid State Commun.*, **77**, 465 (1991).
53) K. Nasu, *J. Phys. Soc. Jpn.*, **53**, 302 (1984).
54) K. Nasu, *J. Phys. Soc. Jpn.*, **53**, 427 (1984).
55) K. Toriumi, Y. Wada, T. Mitani, S. Bandow, M. Yamashita, and Y. Fujii, *J. Am. Chem. Soc.*, **111**, 2341 (1989).
56) K. Toriumi, H. Okamoto, T. Mitani, S. Bandow, M. Yamashita, Y. Wada, Y. Fujii, R. J. H. Clark, D. J. Michael, A. J. Edward, D. Watkin, M. Kurmoo, and P. Day, *Mol. Cryst. Liq. Cryst.*, **181**, 333 (1990).
57) J. Zaanen, G. A. Sawatzky, and J. W. Allen, *Phys. Rev. Lett.*, **55**, 418 (1985).
58) K. Toriumi et al., private communications.
59) N. Matsumoto, M. Yamashita, I. Ueda, and S. Kida, *Mem. Fac. Sci., Kyushu Univ. Sect. C*, **C11**, 209 (1978).
60) K. Toriumi, M. Yamashita, S. Kurita, I. Murase, and T. Ito, *Acta Crystallogr., Sect. B*, **B49**, 497 (1993).
61) H. Endres, H. J. Keller, R. Martin, H. N. Gung, and U. Traeger, *Acta Crystallogr., Sect. B*, **B35**, 1885 (1979).
62) A. L. Beauchamp, D. Layek, and T. Theophanides, *Acta Crystallogr., Sect. B*, **B38**, 1158 (1982).
63) M. Yamashita, K. Toriumi, and T. Ito, *Acta Crystallogr., Sect. C*, **C41**, 876 (1985).
64) K. Toriumi, M. Yamashita, and I. Murase, *Chem. Lett.*, **1986**, 1753.
65) K. Okaniwa, H. Okamoto, T. Mitani, K. Toriumi, and M. Yamashita, *J. Phys. Soc. Jpn.*, **60**, 997 (1991).
66) L. Pauling, "The Nature of the Chemical Bond," 3rd ed, Cornell Univ. Press, Ithaca (1960).
67) O. Muller and R. Roy, "The Major Ternary Structural Families," Springer-Verlag, New York (1974).
68) R. D. Shannon and C. T. Prewitt, *Acta Crystallogr., Sect. B*, **B25**, 925 (1969).
69) Y. Wada et al. previously reported the values of E_{CT} and E_{Im} for No. 2, No. 4, and No. 7 in Ref. 6. According to that, E_{CT} = 2.72 eV and E_{Im} = 1.22 eV for No. 2, E_{CT} = 1.95 eV and E_{Im} = 0.76 eV for No. 4, and E_{CT} = 1.37 eV and E_{Im} = 0.60 eV for No. 7.
70) Y. Wada et al. previously reported in Ref. 15 that E_{Im} = 1.56 eV for No. 13.
71) Y. Wada et al. previously reported in Ref. 15 that E_{CT} = 1.74 eV and E_{Im} = 1.06 eV for No. 14.
72) G. Whitfield and P. B. Shaw, *Phys. Rev.*, **B14**, 3346 (1976).
73) M. Pope and C. E. Swenberg, "Electronic Processes in Organic Crystals," Oxford University Press, Oxford (1982), p. 456.
74) G. B. Blanchet, C. R. Fincher, T. C. Chung, and A. J. Heeger, *Phys. Rev. Lett.*, **50**, 1938 (1983).
75) We previously reported the excitation profiles of PA signals of Pt–I–Pt, Pt–Br–Pt–I, and Pt–Br–Pt–II in Ref. 31. In Ref. 31, we didn't correct the data by taking account of the absorption coefficients. Therefore, the excitation profiles in Ref. 31 are different from those presented in this paper.
76) S. Ichinose, *Solid State Commun.*, **50**, 137 (1984).
77) Y. Onodera, *J. Phys. Soc. Jpn.*, **56**, 250 (1987).
78) D. Baeriswyl and A. R. Bishop, *J. Phys. C*, **21**, 339 (1988).
79) S. Kurita and M. Haruki, *Synth. Met.*, **29**, F129 (1989).
80) N. Kuroda, M. Sakai, M. Suezawa, Y. Nishina, and K. Sumino, *J. Phys. Soc. Jpn.*, **59**, 3049 (1990).
81) M. Sakai, N. Kuroda, M. Suezawa, Y. Nishina, K. Sumino, and M. Yamashita, *J. Phys. Soc. Jpn.*, **61**, 1326 (1992).
82) N. Kuroda, M. Ito, Y. Nishina, A. Kawamori, Y. Kodera, and T. Matsukawa, *Phys. Rev.*, **B48**, 4245 (1993).
83) X. Wei, B. C. Hess, and Z. V. Vardeny, *Phys. Rev. Lett.*, **68**, 666 (1992).
84) A. Terai, in "Relaxation in Polymers," ed by T. Kobayashi, World Scientific, (1993), p. 269.
85) H. Okamoto et al., unpublished results.
86) S. Kivelson and W.-K. Wu, *Phys. Rev.*, **B34**, 5423 (1986).
87) J. Takimoto and M. Sasai, *Phys. Rev.*, **B39**, 8511 (1989).
88) A. Kawamori, R. Aoki, and M. Yamashita, *J. Phys.*, **C18**, 5487 (1985).
89) M. Haruki, M. Tanaka, and S. Kurita, *Synth. Met.*, **19**, 901 (1987).
90) H. Okamoto et al., unpublished results.

Hiroshi Okamoto was born in 1961 in Tokyo, Japan. He received his B. Eng. degree in 1983, M. Eng. in 1985 and D. Eng. in 1988 from University of Tokyo. He joined Institute for Molecular Science as a research associate in 1988. He was appointed as lecturer of Research Institute for Scientific Measurements, Tohoku University in 1992, and he was promoted as associate professor in 1995 in the same institute. He was appointed as associate professor in 1998 in University of Tokyo. His current interests include solid state physics, especially optical, magnetic and magneto-optical properties of transition metal compounds and semiconductors.

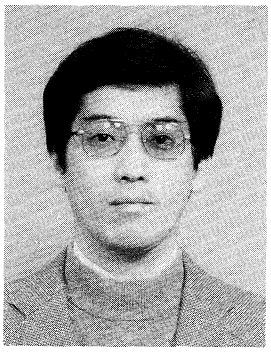

Masahiro Yamashita was born in 1954 at Karatsu in Saga, Japan. He received his B. Sc. degree in 1977, M. Sc. in 1979, and D. Sc. in 1982 from Kyushu University. After his graduation, he joined the Institute for Molecular Science. In 1985, he was appointed as assistant Professor at Kyushu University. In 1989, he was appointed as associate professor at Nagoya University, and he was promoted as full professor in the same university in 1998. Now he is also working at Precursory Research for Embryonic Science and Technology (PRESTO), Japan Science and Technology Corporation (JST). His current interests include the solid state science of the low-dimensional coordination compounds.